Equivalent Circuit Model of Traveling-Wave Maser Slow-Wave Structures

J. Shell
Radio Frequency and Microwave Subsystems Section

An approach is presented for deriving transmission line equivalent circuits that can approximately model the S-parameter response of traveling-wave maser slow-wave structures. The technique is illustrated by computing the S-parameter responses of an X-band and S-band maser slow-wave structure and comparing these with experimental measurements.

I. Introduction

Since the early days of maser development, the traveling-wave maser (TWM) has been widely used because of its small size and its potential for relatively large instantaneous bandwidth, as compared with cavity masers. Several different slow-wave structure (SWS) geometries have been used, including meander lines, quarter-wavelength resonant lines, and half-wavelength resonant lines. One feature they all have in common is the use of predominantly transverse electromagnetic (TEM) resonators placed parallel to one another and coupled by their mutual capacitance and inductance.

Further developments in this area, including new resonant conductor geometries and impedance-matching networks that transition between the SWS and conventional transmission lines, would be enhanced by the use of an approximate equivalent circuit model for the SWS. The purpose of this article is to present one approach to arriving at such approximate equivalent circuits. Equivalent circuits provide a nice physical picture of the SWS and describe well its "filter" behavior: such properties as the upper and lower cutoff frequencies and the group delay. The computational time required to analyze a given structure is generally on the order of minutes, rather than hours or days, as required by many numerical procedures that compute the electromagnetic fields. Predicting the filter properties from an equivalent circuit is a logical first step in the design process. Ultimately, the electromagnetic fields must be calculated to ascertain other properties of the maser, such as the polarization of the signal and pump radio frequency (RF) magnetic fields inside the structure. However, this is best done when the choice of SWS geometries has already been narrowed from consideration of their filter behavior.

This article is organized into eight sections. Following the Introduction, Section II discusses what is required to predict the behavior of coupled-line circuits. Section III describes the SWS geometries that one can consider and some assumptions used in deriving an equivalent circuit. Section IV discusses the solution of the electrostatic field problem, which is necessary to calculate the capacitance matrix. Section V discusses the estimation of the effective dielectric constant, line lengths, and phase velocity. Section VI discusses one way of estimating the terminat-

ing line capacitances. Section VII presents two examples of the analysis: the current JPL X-band (8.45 GHz) half-wavelength comb SWS (Block IIA) and an S-band (2.3 GHz) quarter-wavelength comb SWS partially loaded with ruby. Part VIII presents some discussion and conclusions. Appendix A presents a few other equivalent circuits for representing coupled lines. Appendix B contains a listing of the TOUCHSTONE programs used for the examples in Section VII.

II. Coupled-Line Circuit Theory

Distributed elements, such as transmission lines, obey equations similar to ordinary reactances under certain circumstances. This requires the introduction of a new frequency variable $S = j\tan(\pi f/(2f_0))$. If f_0 is the frequency at which the line is a quarter-wavelength long, then $\pi f/(2f_0)$ is the electrical length of the line.

Consider the input impedance at one end of a transmission line, with the other end short-circuited. The input impedance is given by

$$Z_{in} = jZ_0 \tan\theta \tag{1}$$

where θ is the electrical length of the line. Rewritten in terms of the variable S, this equation is simply

$$Z_{in} = SZ_0 \tag{2}$$

The analogy with the impedance of a conventional inductor, $Z = j\omega L$, leads one to associate L with Z_0, and S with $j\omega$.

If the other end of the line is terminated in an open circuit, the input impedance is given by

$$Z_{in} = -jZ_0 \cot\theta \tag{3}$$

Rewritten in terms of the variable S, this equation is simply

$$Z_{in} = Z_0/S \tag{4}$$

The analogy with the impedance of a conventional capacitor, $Z = 1/(j\omega C)$ leads one to associate C with $1/Z_0$, and S with $j\omega$.

The impedance of a TEM transmission line is uniquely given by its static capacitance/unit length as

$$Z_0 = 1/(V_p C_{\text{static}}) = \frac{377 \text{ ohms}}{\sqrt{\epsilon_r} C_{\text{static}}/\epsilon_0} \tag{5}$$

where V_p is the phase velocity, 377 ohms is the impedance of free space, ϵ_r is the relative dielectric constant, and ϵ_0 is the permittivity of free space. The static capacitance network provides the connection between the field solution and the conductor geometry. It is not an equivalent circuit. The equivalent circuit is obtained by applying the relevant boundary conditions to the admittance or impedance matrix description of the coupled lines. This results in a set of equations that relate the static capacitance values to the L's, C's, and unit elements of the equivalent circuit. Again, the L's are a shorthand notation for shorted transmission lines and the C's are a shorthand notation for open-circuited lengths of transmission line.

When the problem is generalized to coupled lines, the voltage and current become two component vectors. They are related by

$$\frac{dV}{dz} = -j\omega LI \qquad \frac{dI}{dz} = -j\omega CV \tag{6}$$

where L and C are 2-by-2 matrices. C is given by

$$C = \begin{bmatrix} C_1 + C_m & -C_m \\ -C_m & C_2 + C_m \end{bmatrix} \tag{7}$$

Here, C_m is the mutual capacitance/unit length between the lines, and C_1 is the self capacitance/unit length between line 1 and the ground. Since a TEM line has a unique propagation velocity, the matrix product LC is diagonal, where the diagonal elements are just the square of the phase velocity. Therefore, the capacitances and the phase velocity are all one needs to know to describe the coupled lines.

Since the distributed capacitance/unit length between a line and its ground plane (and the phase velocity) can describe a TEM transmission line, it seems reasonable that the distributed mutual capacitance/unit length between two lines might also describe a transmission line. This approach has been developed and yields the three-line equivalent circuit for coupled TEM lines, shown in Fig. 1, as described by Seviora [1].

This article uses a different equivalent circuit to represent the coupled lines. (A few more alternative equivalent circuits are given in Appendix A.) The equivalent circuit chosen for this article was originally developed by Sato and Cristal [2]. (See Fig. 2; the bottom portion of the figure is the shorthand notation used in this article. Shorted lengths of transmission line are written as inductors, and the ground planes or return conductors are omitted.) The reader may notice that the transmission lines running diagonally have negative impedance. The S parameters of a negative characteristic impedance line are the complex conjugate of those of the positive impedance line. As long as the network analysis program correctly accounts for this, such negative impedances are not a problem.

In this article, all the "inductors" are shorted lengths of transmission line. Some of the "capacitors" here are capacitances/unit length and represent a distributed coupling that is modeled as a transmission line. However, the fringing capacitances discussed here are of the ordinary, lumped variety, and this mixture of capacitor types should be kept in mind by the reader.

To summarize, the static capacitance matrix is central to the theoretical description of microwave filters using parallel coupled lines. It serves a dual purpose. From the microwave viewpoint, the capacitance represents the distributed coupling between two lines, or between a line and a ground plane. A proper network description of this coupling requires familiarity with Richard's transformation and the Kuroda transformations. This article will not derive the network-equivalent circuit but will take it as given. From the physical viewpoint, the capacitances represent the usual capacitance found by solving the electrostatic field problem. The physical basis of the dual function of the static capacitance is a somewhat subtle idea, which involves the use of complex potentials [3], and will not be explored further here.

The original derivation of the impedance matrix for coupled lines was done by Jones and Bolljahn [4]. Riblet [3] put the admittance description on firm theoretical ground. An important set of papers by Wenzel [5–8] provides a good introduction to capacitance matrices and coupled-line theory.

III. Possible SWS Transverse Geometries and Assumptions

The range of SWS transverse (the cross-sectional view normal to the lengths of the lines) geometries that can be analyzed is large, if the program which calculates the capacitance matrix is of sufficient generality. The recent availability of software (hereafter denoted by MPMCTL) developed by workers at Syracuse University [9] enables a wide range of geometries to be considered. MPMCTL is written explicitly to handle the transverse geometries shown in Fig. 3. These include (a) infinitely thin coupled microstrips, (b) finite thickness coupled microstrips, (c) coupled suspended substrate striplines, (d) coupled rectangular conductors, (e) coupled striplines, (f) broadside coupled lines, and (g) a coplanar waveguide. However, user-defined geometries are also available. Multiple dielectric layers are allowed if the dielectric interfaces are parallel to the ground planes.

Since the analytic description is based on a two-dimensional static capacitance matrix, it implicitly assumes TEM-mode propagation. If the conductors are parallel to the ground planes and embedded in a material with a uniform dielectric constant, then it is a good assumption that the waves excited on the lines are TEM waves. If the dielectric loading is not homogeneous, the fields are not pure TEM. However, in that case, this article will calculate an effective homogeneous dielectric constant and continue to assume TEM-mode propagation.

Besides a homogeneous dielectric constant, the largest cross-sectional dimension of the line must be small, as compared with a wavelength, so that the axial components will be small, as compared with the transverse components, and the wave essentially TEM. If the lines are close together, as compared with a wavelength, one may neglect retardation effects as well.

The approach taken in the analysis is the following. The impedances of all the transmission lines in the equivalent circuit are determined from the static capacitance matrix (calculated using MPMCTL) for that line geometry. The electrical length of the lines is determined from the known physical length and the effective dielectric constant. The terminating reactances are calculated separately. For fringing capacitances, the author uses the published results of Getsinger [10]. The S-parameters of the final equivalent circuit are calculated with a microwave computer-aided design (CAD) program called TOUCHSTONE [11].

IV. Solution of the Electrostatic Field Problem

The static capacitance matrix discussed in Section III is obtained by solving the two-dimensional Laplace equation for the static electric field for the given arrangement of conductors (assuming that the conductors are infinite

in length). There are several approaches to solving such boundary value problems. The approaches will not be discussed in detail, because they are covered extensively in the literature. Nevertheless, a few remarks are in order.

Conformal mapping has been used to obtain exact results when there are two conductors symmetrically placed between ground planes [12]. If they are unsymmetrically placed, the analysis becomes very unwieldy. The numerical approaches are able to handle a larger number of conductors than the analytical approaches. This is especially important if next-nearest-neighbor coupling is significant. The finite difference-equation approach has been extensively used [13], but it requires more computer time than other techniques and, unless a very fine mesh is used, is generally not extremely accurate. Its primary advantage is the simplicity of the algorithm.

The most accurate results, especially for edge-coupled striplines, have been obtained by using a Green's function integral equation moment method. This moment method can give accuracies of a few tenths of a percent [14]. The calculation of the capacitance matrix using such a method was carried out by Kammler [15]. This approach is general enough to handle any number of conductors; however, it is restricted to very thin conductors that are parallel to the ground planes and embedded in a homogeneous dielectric medium. The current JPL X-band masers (Block IIA) satisfy these restrictions quite well. A FORTRAN program based on Kammler's algorithm was written and used by the author to model the X-band maser prior to the appearance of MPMCTL.

The MPMCTL software uses a free-space Green's function integral equation formalism [16]. The dielectric is replaced by the equivalent bound charge densities. The equations are solved by using a moment method that gives good agreement with the author's program in the geometries common to both. MPMCTL also gives the charge densities on each pulse. MPMCTL is general enough to handle losses, although that capability is not used for this article. Further improvements to the model will include this.

V. Effective Dielectric Constant, Relative Velocity, and Line Length

The effective relative dielectric constant can be regarded as the ratio of the charges on a given conductor with partial dielectric loading to the ratio of the charges on the same conductor when there is no dielectric, provided that the potentials of the conductor are the same in both cases. Since the capacitance is the charge per unit voltage, if one assumes always a voltage of 1 V, the elements of the capacitance matrix give the charges on the conductors. That is, C_{ij} is the charge on conductor i if conductor j is at a potential of 1 V and all other conductors are grounded.

It is particularly easy to determine the effective dielectric constant at the lower cutoff frequency, the midband frequency, and the upper cutoff frequency, since the voltage distribution on the conductors is simple. At the lower cutoff frequency, all the conductors are at the same potential (for example, 1 V). At midband, the voltage progresses from finger to finger as +1 V, 0 V, −1 V, 0 V, +1 V, etc. At the upper cutoff frequency the voltage progresses as +1V, −1 V, +1 V, −1 V, etc. (See Fig. 4.)

Consider the following example. If one has three conductors, as shown in Fig. 4(a), then the charge on conductor 2 (i.e., Q_2) equals C_{21} plus C_{22} plus C_{23}. Note that C_{21} and C_{23} are negative, that is, a 1-V potential on fingers 1 and 3 induces a negative charge on finger 2. A 1-V potential on finger 2 induces a positive charge on finger 2. The total charge on finger 2 is the algebraic sum of the charges.

If the three conductors are at midband, Fig. 4(b), then the charge on finger 2 is given by C_{22} alone, because fingers 1 and 3 at 0 V do not induce any charge on finger 2. Therefore, Q_2 equals C_{22}.

If the three conductors are at the upper cutoff frequency, Fig. 4(c), then the negative potential of fingers 1 and 3 induces a positive charge on finger 2, which adds to the positive charge induced by finger 2 being at 1 V. Therefore, Q_2 equals $|C_{21}|$ plus C_{22} plus $|C_{23}|$.

This is repeated for the partially loaded geometry, and the effective relative dielectric constant is given by the ratio of Q_2 in the loaded and unloaded cases. That is, ϵ_{eff} equals $Q_2(\text{loaded})/Q_2(\text{empty})$.

Once the effective dielectric constant is known, the phase velocity is equal to $c/\sqrt{\epsilon_{\text{eff}}}$, where c is the speed of light in a vacuum. An estimate for the electrical length of the fingers in degrees can now be found from

$$\theta = (360 f l_p)/V_p \tag{8}$$

where f is the frequency, l_p is the physical length, and V_p is the phase velocity in the medium of propagation. Determining this line length is necessary for the equivalent

circuits. The physical length is known from the geometry of the structure.

VI. Terminating Reactances

The masers built at JPL generally use a capacitive loading on one or both ends of the fingers. The capacitances used in practice are very small, on the order of tenths of picofarads. Although these capacitances are small, they play a vital role. One might guess that a finger a full half-wavelength long, with no terminating capacitance, could also serve as a possible SWS geometry. However, in this case, the capacitive coupling between the lines exactly balances the magnetic coupling, and there is no propagation down the SWS. The capacitive loading at the ends of the fingers is necessary to upset the balance.

Another way to see this is to examine the Poynting vector. The transverse E and H fields account for the propagation of energy back and forth along the finger. They do not lead to energy propagation from finger to finger down the SWS. The component of the fringing electric field along the length of the finger (see Fig. 5) and the magnetic field perpendicular to the length of the finger cause a component of the Poynting vector to be directed down the structure.

To model SWS's, one must estimate the capacitive loading from the fingertips to the surrounding copper walls. This capacitance is generally some combination of parallel plate capacitance and fringing capacitance. (A fringing capacitance accounts for the electric field lines that are not straight and uniform between the conductors, but rather tend to bulge near the ends.) There are two fingertip loading capacitances that must be estimated; they are shown in Fig. 6. The first, designated C_f, is the capacitance from the end of the finger to the surrounding walls. The second, designated C_x, is the capacitance from the end of one finger to the end of an adjacent finger.

It should be mentioned that these capacitances will depend on the frequency within the passband of the SWS. For example, at the lower cutoff frequency, all the fingers are at the same potential. The electric field has no normal component at the plane midway between the fingers. Therefore, C_x must be zero at the lower cutoff frequency. At the upper cutoff frequency, adjacent fingers are at opposite potential, and the electric field has only a normal component at the plane midway between the fingers. Here C_x must be maximum. This article assumes that C_f and C_x are independent of the frequency. The purpose of this section is to show how to obtain ballpark estimates of the capacitances for use in the equivalent circuits. Further refinements would include more exact calculations, as well as the frequency dependance.

The values of the fringing capacitances can be estimated with the results obtained by Getsinger for rectangular conductors centered between ground planes. The capacitances that Getsinger calculates are shown in Fig. 7. The odd-mode fringing capacitance, C'_{f0}, is the capacitance per unit length to ground (this includes the top and bottom ground planes, as well as the end wall) from one corner and half the associated vertical wall in the coupling region for a bar with odd-mode excitation. The even-mode-fringing capacitance, C'_{fe}, is the capacitance per unit length to ground (in this case, only the top and bottom planes) from one corner and half the associated vertical wall in the coupling region of a bar with even-mode excitation. Getsinger determined the capacitances by using a conformal mapping technique. The results are exact for bars extending in width infinitely far from the coupling region between the conductors. (Future CAD work may benefit from expressions derived by Perlow [17], which provide relatively simple algebraic expressions for the coupling capacitances, in place of Getsinger's charts.)

In order to estimate C_f, use Getsinger's values of $C'_{f0}(s/b, t/b)$, where s is twice the gap (g) between the end of the finger and the opposing ground plane. See Fig. 8. Since the capacitances are per unit length, multiply by the width w of the conductor. Since Getsinger's charts are for centered conductors, estimate C_f by adding the capacitances for the two cases of different b. (The capacitances are added because each one gives the contribution from only half of the vertical wall at the end of the finger.) This gives the fringing capacitance from a horizontal edge as

$$C_f = \epsilon w \left\{ \frac{C'_{f0}}{\epsilon} \ (2g/b_1, t/b_1) + \frac{C'_{f0}}{\epsilon} (2g/b_2, t/b_2) \right\} \quad (9)$$

where ϵ, equal to $\epsilon_0 \ \epsilon_r$, is the dielectric permittivity of the medium. Here ϵ_0, equal to 0.0886 pF/cm, is the permittivity of free space, and ϵ_r is the relative dielectric constant.

The finger-to-finger fringing capacitance C_x can be estimated from Getsinger's charts if one uses C'_{fe} and the geometry of Fig. 9. Now the spacing between the ground planes is the pitch p of the slow-wave structure. The width of the fingers w (as used above) now plays the role of Getsinger's t and vice versa. Thus, one obtains

$$C_x = \epsilon t \frac{C'_{fe}}{\epsilon} (2g/p, w/p) \quad (10)$$

There is no factor of 2 here because in the equivalent circuits one has two capacitors C_x leaving each fingertip. The values obtained in this way can be used as starting values for the models.

VII. Examples

A. X-Band Half-Wavelength Comb

The geometry of the current X-band Block IIA SWS is shown in Fig. 10. If one starts with the equivalent circuit of Sato and Cristal, this will model the coupling between the fingers. The nodes at the ends of the transmission lines in the equivalent circuit correspond to the ends of the fingers. The 12-mil gap between the ends of the fingers and the copper cavity (ground) is represented by a fringing capacitance C_f. The electric field between the ends of the fingers is represented by a fringing capacitance, C_x.

The capacitance matrix for an array of five conductors with the geometry of Fig. 10(a) can be calculated with MPMCTL and is given by

$$[C] = \begin{bmatrix} 272.2 & -43.04 & -3.996 & -0.876 & -0.265 \\ -43.04 & 280.8 & -42.27 & -3.83 & -0.877 \\ -3.99 & -42.27 & 280.8 & -42.27 & -3.99 \\ -0.876 & -3.83 & -42.27 & 280.8 & -43.04 \\ -0.266 & -0.877 & -3.99 & -43.04 & 272.2 \end{bmatrix} \text{ pF/m} \tag{11}$$

The self and mutual capacitances of the parallel conductors are easily derived from the capacitance matrix. C_{self} is given by

$$\left.\begin{aligned} C_{\text{self}} &= -3.99 - 42.27 + 280.8 - 42.27 - 3.99 \\ &= 188.28 \text{ pF/m} \\ C_{\text{mut}} &= 42.27 \text{ pF/m} \end{aligned}\right\} \tag{12}$$

The line admittances are given by

$$Y_{\text{self}} = V_p C_{\text{self}} = \frac{(3 \times 10^8)\,(188.28 \times 10^{-12})}{\sqrt{9.8}}$$

$$= 1.80 \times 10^{-2} \text{ mhos} \tag{13}$$

or $Z_{\text{self}} = 1/Y_{\text{self}} = 55.5$ ohms

$$Y_{\text{mut}} = \frac{(3 \times 10^8)\,(42.27 \times 10^{-12})}{\sqrt{9.8}} = 4.05 \times 10^{-3} \text{ mhos} \tag{14}$$

or $Z_{\text{mut}} = 1/Y_{\text{mut}} = 247$ ohms.

The line lengths are easily determined because the dielectric filling is assumed to be uniform. For the X-band maser, the finger length of 0.196 in., see Fig. 10(b), corresponds to an electrical length of 150 deg at 8 GHz.

Finally, the fringing capacitances are determined. Using values of g equal to 0.012 in., s equal to 0.024 in., b_1 equal to 0.080 in., b_2 equal to 0.220 in., t equal to 0.002 in., ϵ_0 equal to 0.0886 pF/cm, w equal to 0.040, $\epsilon_r = 9.8$, and Getsinger's charts, one calculates C_f equal to 0.19 pF. By using g equal to 0.012 in., p equal to 0.080 in., t equal to 0.040 in., w equal to 0.002 in., ϵ_0 equal to 0.0886 pF/cm, ϵ_r equal to 9.8, and Getsinger's charts, one calculates C_x equal to 0.01 pF.

The equivalent circuit for five fingers is shown in Fig. 11. The author finds that better agreement with measured data is obtained if C_f is decreased slightly to 0.1 pF, and C_x is changed to -0.005 pF. A calculation of S_{21} for this circuit with the new values using TOUCHSTONE is given in Fig. 12. The measured behavior of S_{21} for a comb with 44 fingers is shown in Fig. 13. The predicted group delay for five fingers is shown in Fig. 14. At midband, the delay is about 1 nsec. Therefore, for 44 fingers one would expect about 8.8 nsec. The measured group delay is shown in Fig. 15 and is about 9 nsec at midband.

B. S-Band Quarter-Wavelength Comb

In this example, the basic approach used above can be generalized to handle more complicated structures. The example chosen is an S-band quarter-wavelength comb structure with ruby loading on one side of the fingers, and no dielectric on the other side. The dielectric does not extend along the entire length of the finger. The geometry is shown in Fig. 16. A similar geometry is being considered for a Ka-band (32-GHz) traveling-wave maser.

The problem naturally lends itself to a two-part analysis. The first part begins at the bottom of the cavity, where the fingers are shorted, and extends to the point on the fingers where the dielectric stops. The second part begins at the top of the dielectric and extends to the cover.

The first part can be thought of as a conventional comb structure, with the additional complication of partial dielectric loading. The first task is to derive an equivalent circuit for the comb structure by starting from the basic circuit of Sato and Cristal. Then the capacitance matrix is calculated as before, by using MPMCTL. The capacitance matrix will also be calculated for the empty comb, which is necessary in order to model the unloaded portion of the comb, as well as to calculate the effective dielectric constant. The line admittances will be derived from the elements of the first capacitance matrix as before, except that the velocity of propagation will depend on the value of the effective dielectric constant. The effective electrical length of the lines in degrees also depends on this effective dielectric constant. The second part of the circuit will be represented by a Sato/Cristal pair of lines. One set of nodes coincides with the nodes at the top of the dielectric, the other set of nodes is located at the tops of the fingers. As before, the electric field from the fingertips to ground and from fingertip to fingertip is represented by C_f and C_x, respectively.

Starting with the equivalent circuit for a pair of coupled lines, a somewhat simpler circuit results if one end of all the conductors is grounded. The resulting circuit is shown in Fig. 17. One is left with an equivalent circuit composed only of S-plane inductors (i.e., shorted transmission lines).

The capacitance matrix for the finger geometry without any dielectric is obtained by using MPMCTL. The result for three fingers is

$$[C] = \begin{bmatrix} 33.76 & -9.64 & -0.259 \\ -9.64 & 37.42 & -9.64 \\ -0.259 & -9.64 & 33.76 \end{bmatrix} \text{ pF/m} \qquad (15)$$

The capacitance matrix for the section of the structure with partial filling requires more work. The user-defined geometry portion of MPMCTL must be used. The 136 nodes used for the moment method calculation are shown in Fig. 18.

The capacitance matrix for three fingers is calculated to be

$$[C] = \begin{bmatrix} 107.6 & -24.95 & -0.800 \\ -25.02 & 117.1 & -25.00 \\ -0.800 & -24.98 & 107.6 \end{bmatrix} \text{ pF/m} \qquad (16)$$

Therefore, the effective dielectric constants at lower, midband, and upper cutoffs are given by

$$\left.\begin{aligned} \epsilon_{\text{eff}}(\text{lower cutoff}) &= \frac{67.08}{18.13} = 3.70 \\ \epsilon_{\text{eff}}(\text{midband}) &= \frac{117.1}{37.42} = 3.13 \\ \epsilon_{\text{eff}}(\text{upper cutoff}) &= \frac{167.12}{56.7} = 2.95 \end{aligned}\right\} \qquad (17)$$

The line impedances for the empty portion of the comb are determined as before,

$$\left.\begin{aligned} C_{\text{self}} &= -9.64 + 37.42 - 9.64 = 18.14 \text{ pF/m} \\ C_{\text{mut}} &= 9.64 \text{ pF/m} \end{aligned}\right\} \qquad (18)$$

$$\left.\begin{aligned} Y_{\text{self}} &= (3 \times 10^8)\,(18.14 \times 10^{-12}) \\ &= 5.44 \times 10^{-3} \text{ mhos} \\ Z_{\text{self}} &= 1/Y_{\text{self}} = 184 \text{ ohms} \end{aligned}\right\} \qquad (19)$$

$$\left.\begin{aligned} Y_{\text{mut}} &= (3 \times 10^8)\,(9.64 \times 10^{-12}) \\ &= 2.892 \times 10^{-3} \text{ mhos} \\ Z_{\text{mut}} &= 1/Y_{\text{mut}} = 346 \text{ ohms} \end{aligned}\right\} \qquad (20)$$

Similarly, for the partially filled portion of the comb,

$$\left.\begin{aligned} C_{\text{self}} &= -25.02 + 117.1 - 25.00 = 67.08 \text{ pF/m} \\ C_{\text{mut}} &= 25.0 \text{ pF/m} \end{aligned}\right\} \quad (21)$$

$$Y_{\text{self}} = \frac{(3 \times 10^8)\,(67.08 \times 10^{-12})}{\sqrt{3.13}} = 1.1375 \times 10^{-2} \text{ mhos} \quad (22)$$

$$Y_{\text{mut}} = \frac{(3 \times 10^8)\,(25.01 \times 10^{-12})}{\sqrt{3.13}} = 4.2409 \times 10^{-3} \text{ mhos} \quad (23)$$

$$Z_{\text{mut}} = 1/Y_{\text{mut}} = 236 \text{ ohms} \quad (24)$$

$$Y_{\text{self}} - Y_{\text{mut}} = 7.1341 \times 10^{-3} \text{ mhos} \quad (25)$$

$$1/(Y_{\text{self}} - Y_{\text{mut}}) = 140 \text{ ohms} \quad (26)$$

The line lengths are also required. For the unloaded portion of the line, θ equals 16.5 deg at 2 GHz. For the loaded portion, θ equals 47.5 deg.

The fringing capacitances are determined as before. Using $t = 0.050$ in., $s = 0.140$ in., $b = 0.280$ in., $w = 0.050$ in., one finds that $C_f = 0.0214$ pF. For the finger-to-finger fringing capacitance, one uses $t = 0.050$ in., $s = 0.140$ in., $b = 0.125$ in., and $w = 0.050$ in. One then finds that $C_x = 0.01$ pF.

The equivalent circuit for five fingers is shown in Fig. 19. Better agreement with the measured data is obtained if C_x is increased to 0.065 pF and the electrical length of the loaded portion of the fingers is increased to 56 deg. A TOUCHSTONE analysis of this circuit is shown in Fig. 20. The measured data are shown in Fig. 21. The calculated group delay for five fingers is shown in Fig. 22; at midband this is about 2 nsec. Therefore, 48 fingers would be expected to have a group delay of about 19.2 nsec. The measured data are shown in Fig. 23. The group delay is about 20 nsec at midband.

VIII. Discussion and Further Improvements

A summary of the the two examples worked out in Section VII is given in Table 1. The first three rows of the table compare the calculated and measured values of the upper and lower cutoff frequencies (at approximately the −3-dB points) and the group delay at the center of the bandpass. The calculated values are for a five-resonator structure. (The group delay is multiplied by the appropriate factor to make the number of resonators the same in the calculated and measured cases.) The values of the parameters used in the equivalent circuits are shown in the last eight rows of the table. If those values are different from those calculated in Section VII from purely geometrical considerations, the calculated value is given in parentheses next to the value used in the TOUCHSTONE program. Some flexibility was allowed because the theoretical filter response can be a very sensitive function of some parameters whose values are hard to calculate precisely. For example, the bandwidth is a very sensitive function of C_x; if one judged the model solely on the basis of the prediction by using the estimated value for C_x, one might conclude that the overall model is a poor one, when in fact the problem lies in the estimation of C_x.

The values for the line impedances were never adjusted, and only the electrical length for the partially filled portion of the S-band structure was adjusted. The value of 56 deg corresponds to a dielectric constant of about 4.3, which is not too different from the estimated effective dielectric constant of 3.7 at the lower cutoff. Nevertheless, this may be hinting that a more accurate model is really necessary, one which takes into account the quasi-TEM nature of the propagation.

Among the more interesting surprises was the need for a negative finger-to-finger fringing capacitance for the X-band model. The reason for this is still unclear. A positive value here can also give approximately the right bandwidth, but it was found that the negative value matches more nearly the observed overall shape of the group delay response. In particular, the greater slowing at the upper cutoff is predicted with a negative coupling capacitance, whereas a positive capacitance predicts a greater slowing at the lower cutoff.

Parallel coupled strip lines and rectangular conductors in a geometry useful for maser slow-wave structures can be approximately modeled. The models require calculation of the static capacitance matrix of the two-dimensional array of transmission lines, as well as any (reactive) terminations on the ends of the lines. From a knowledge of the capacitance matrix, transmission-line equivalent circuits for the coupled lines can be found. The (reactive) terminations are modeled as lumped elements. Approximate estimates of these terminations may be obtained by using published data, such as Getsinger's [10]. Once the circuit is obtained, the S-parameters can be obtained with a commercially available CAD program, such as TOUCH-

STONE. All the S-parameters can be calculated, as well as the group delay.

Further work in this area would include better calculation of the fringing capacitances, especially the variation of these capacitances with frequency For the inhomogeneous structures, a four-transmission-line equivalent circuit (as is shown in Appendix A) should give better results than the "equivalent dielectric constant" approach used in this article.

Acknowledgments

The author thanks R. J. Wenzel for bringing the work of Sato and Cristal to his attention, and to Professor Sam Derman of the City College of New York for numerous valuable discussions.

Table 1. Summary of X- and S-band SWS parameters

	X-Band		S-Band	
	Measured	Calculated	Measured	Calculated
f_{lower}, GHz	7.3	7.2	2.41	2.44
f_{upper}, GHz	8.4	8.54	2.86	2.90
Delay, nsec	9.0	8.8	20.0	19.2
$Z_1(\Omega)$	55.5		346	
$Z_2(\Omega)$	247		184	
$Z_3(\Omega)$	—		236	
$Z_4(\Omega)$	—		140	
θ_1 (deg)	150		16.5	
θ_2 (deg)	—		56 (47.5)	
C_F(pF)	0.10 (0.19)		0.0214	
C_x(pF)	−0.005 (0.0099)		0.065 (0.01)	

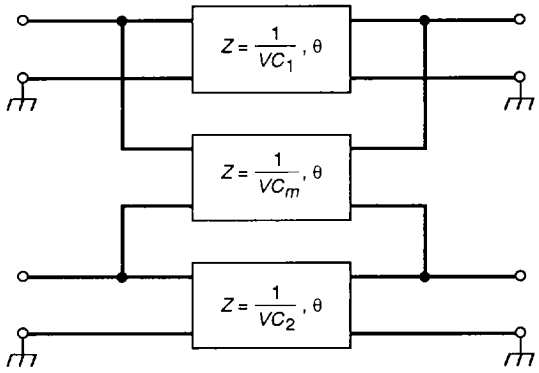

Fig. 1. Three-line equivalent circuit for coupled TEM lines.

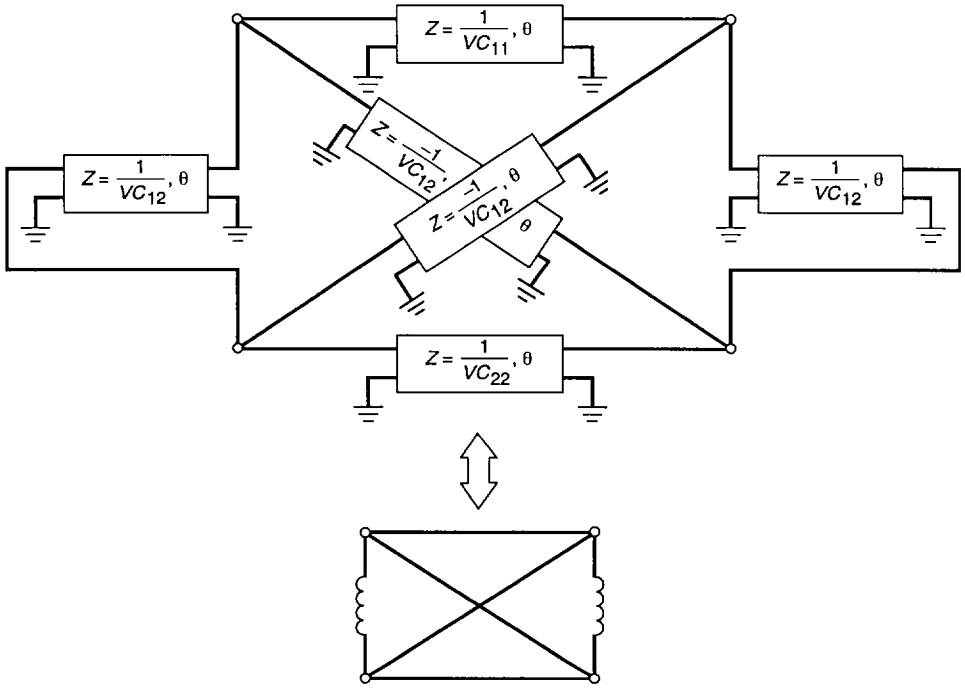

Fig. 2. Six-line equivalent circuit for coupled TEM lines.

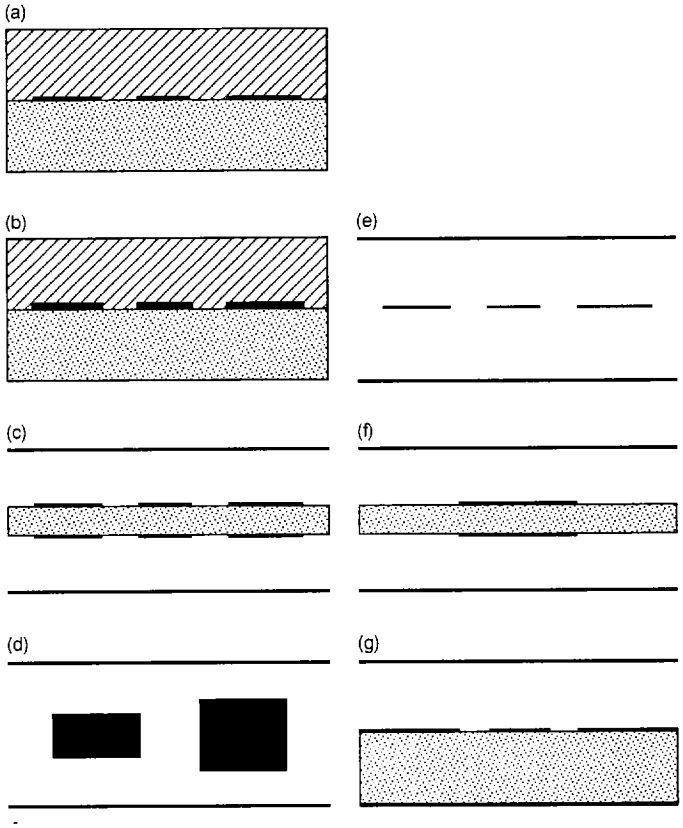

Fig. 3. Transverse geometries that can be handled by MPMCTL.

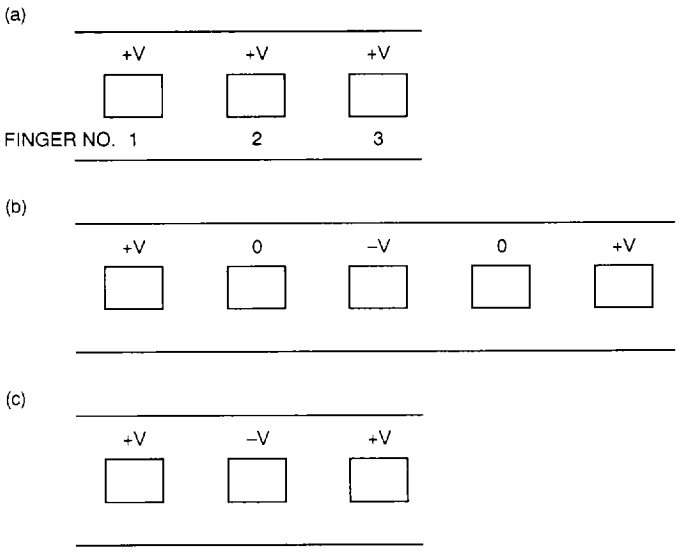

Fig. 4. Voltage distribution along the fingers for various circumstances: (a) at the lower cutoff frequency; (b) at the midband frequency; and (c) at the upper cutoff frequency.

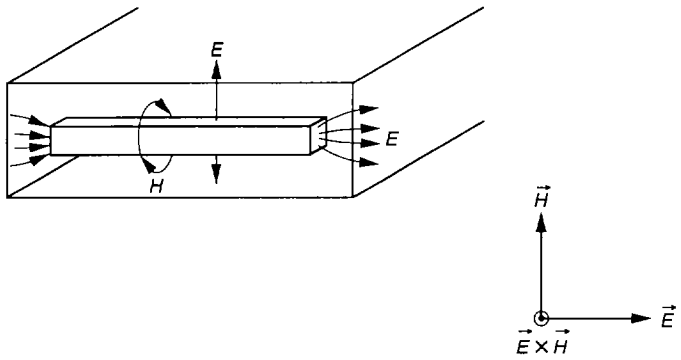

Fig. 5. Electric and magnetic field lines for a half-wavelength finger inside a cavity.

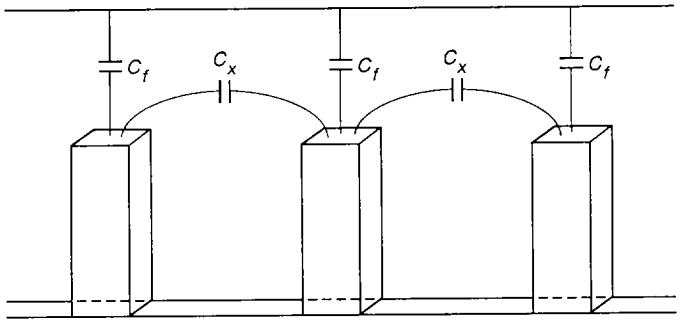

Fig. 6. The fringing capacitances from the ends of the fingers to ground (C_f) and between fingertips (C_x).

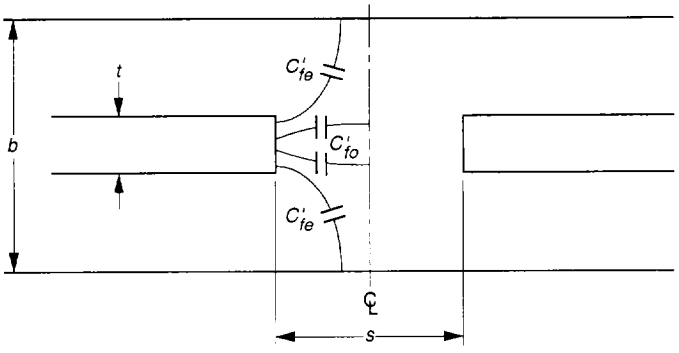

Fig. 7. The even-mode (C'_{fe}) and odd-mode (C'_{fo}) fringing capacitances considered by Getsinger.

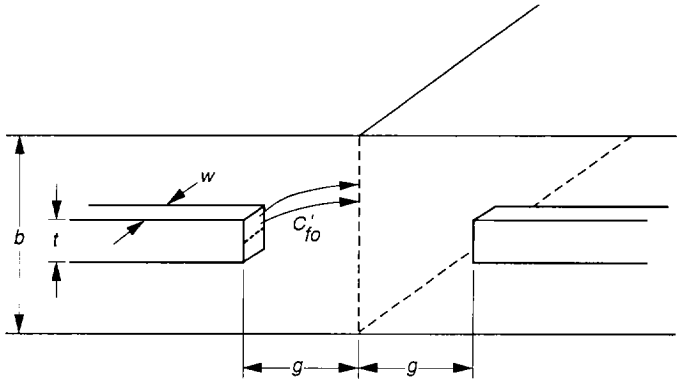

Fig. 8. Geometry used to calculate the fringing capacitance from the ends of the fingers to ground.

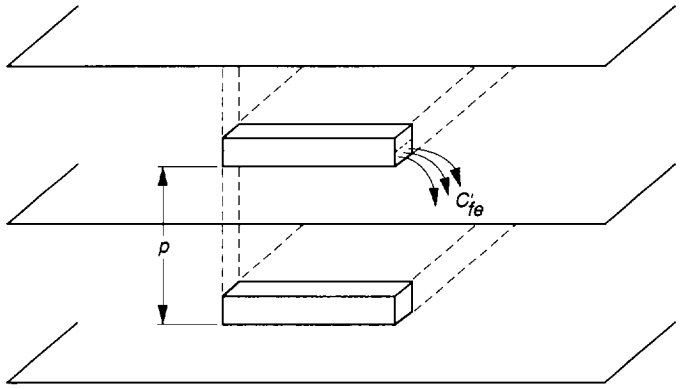

Fig. 9. Geometry used to calculate the fringing capacitance from fingertip to fingertip.

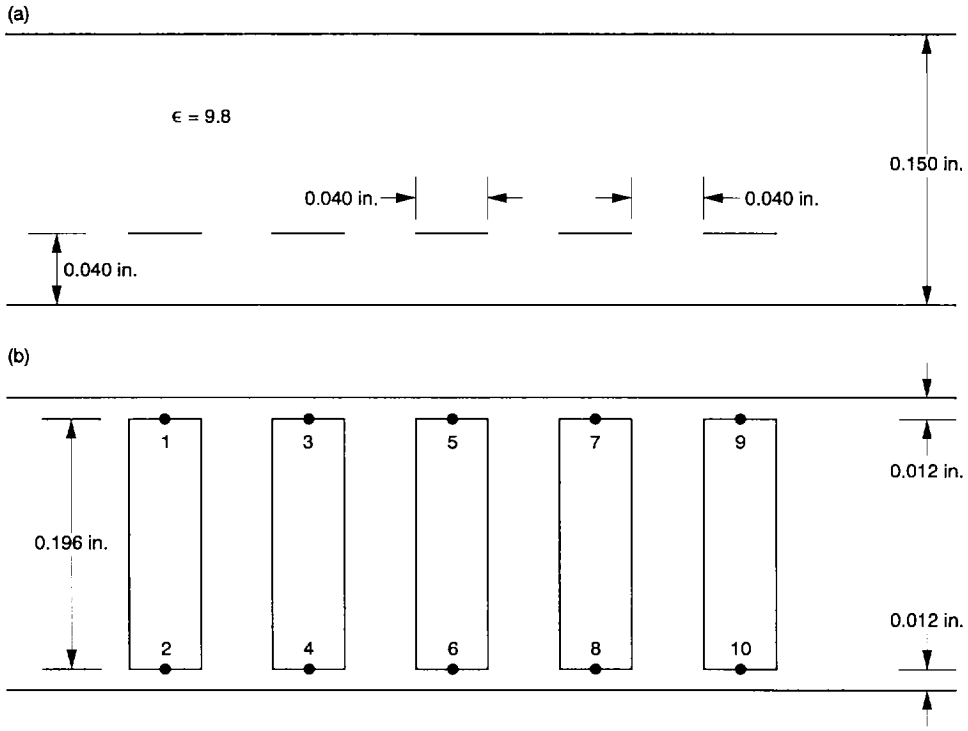

Fig. 10. Geometry of the X-band (Block IIA) slow-wave structure for five fingers: (a) transverse view, and (b) side view.

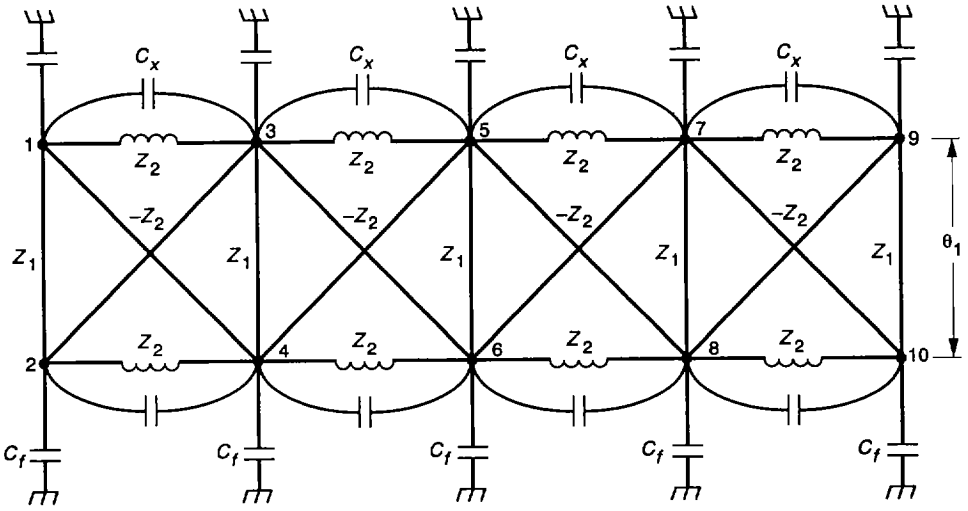

Fig. 11. Equivalent circuit used to model the X-band slow-wave structure of Fig. 10.

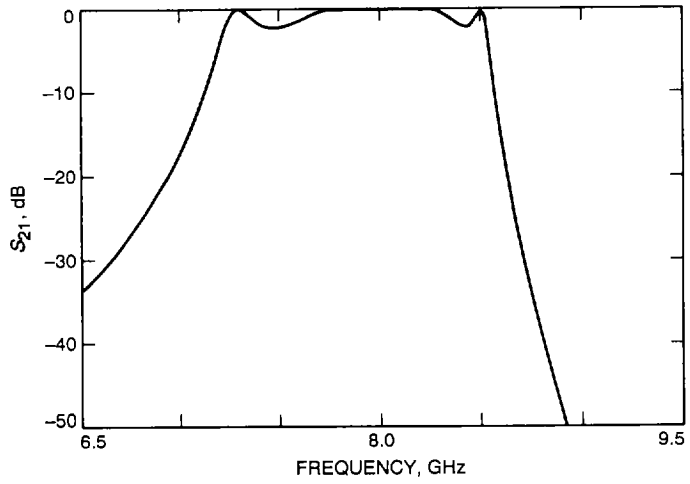

Fig. 12. Calculated S_{21} response for the circuit of Fig. 11.

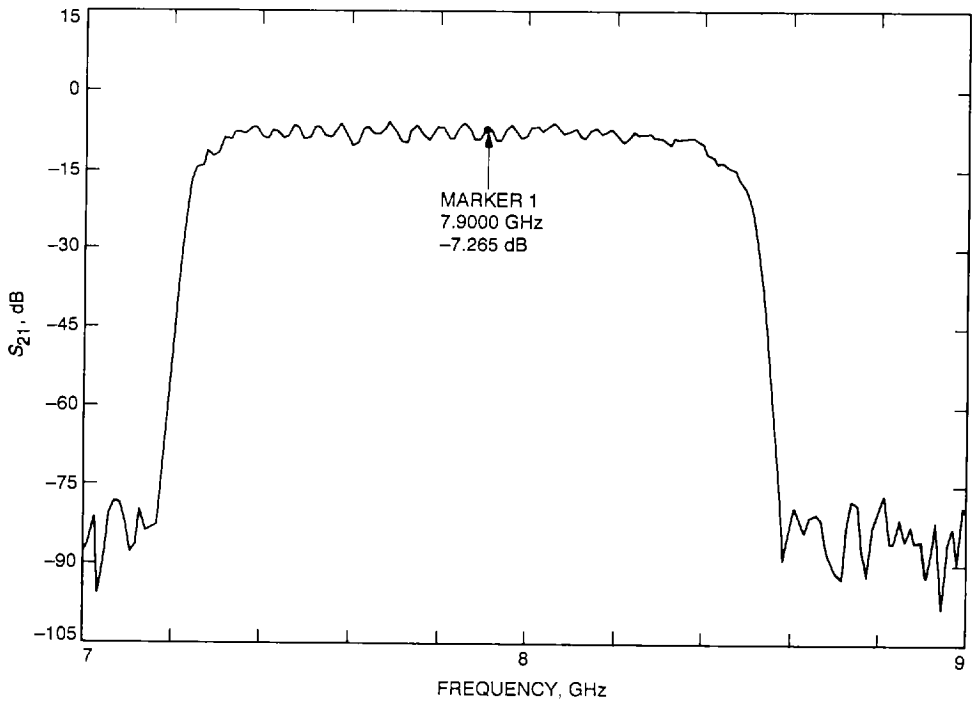

Fig. 13. Measured S_{21} response for the Block IIA slow-wave structure, which contains 44 fingers.

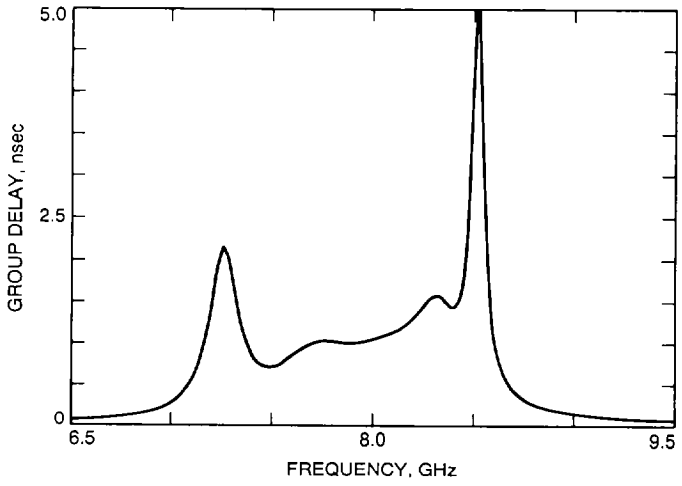

Fig. 14. Calculated group delay for the circuit of Fig. 11.

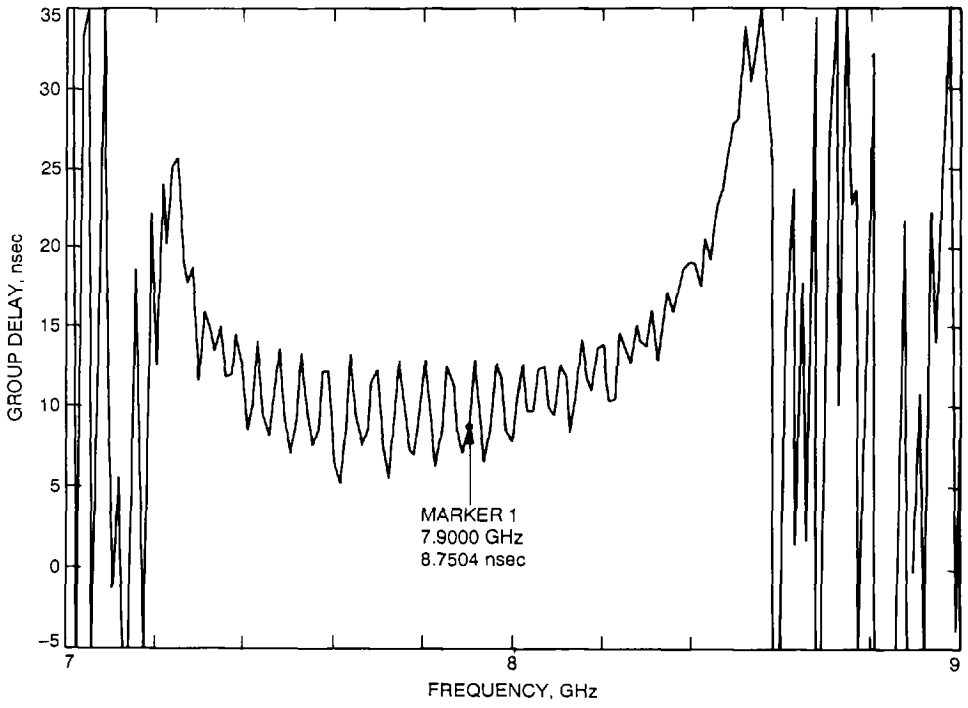

Fig. 15. Measured group delay for the Block IIA slow-wave structure.

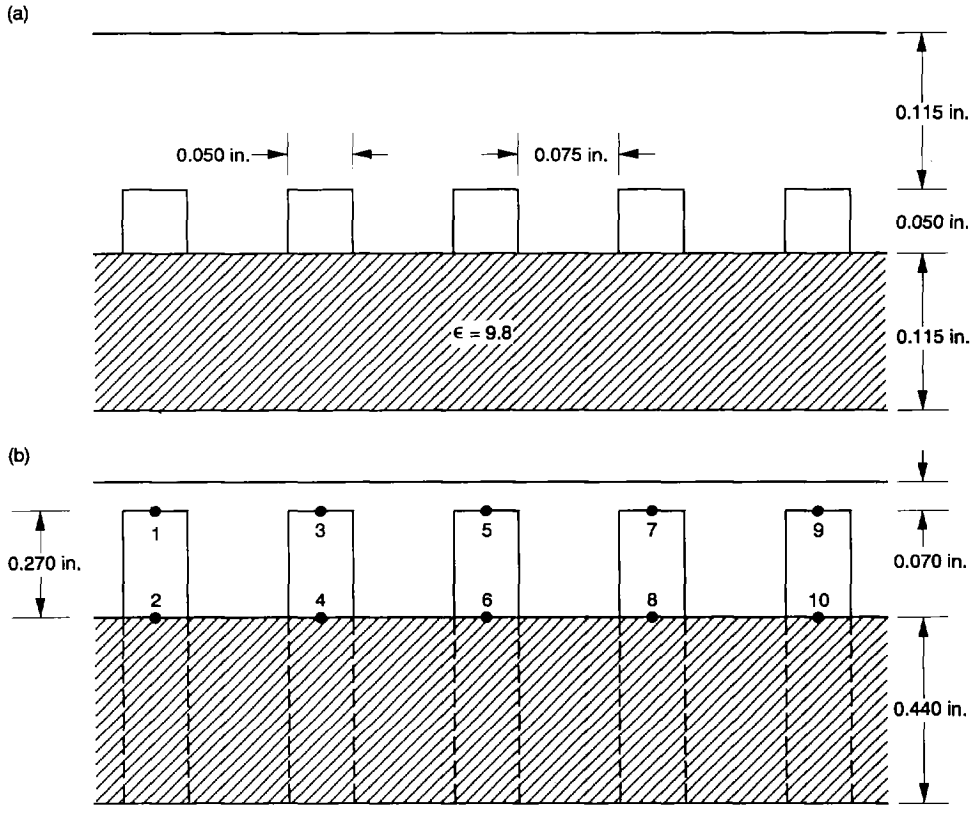

Fig. 16. Geometry of the partially loaded S-band slow-wave structure for five fingers: *(a) transverse view, and (b) side view.*

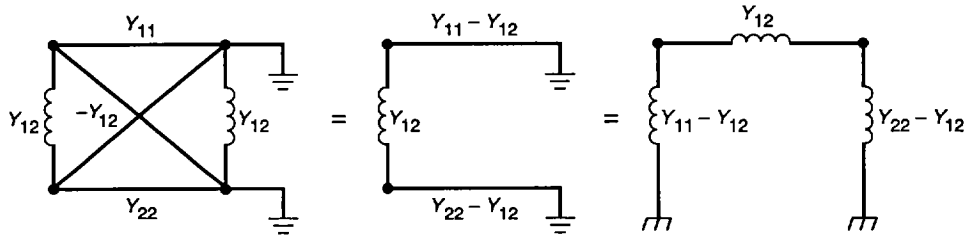

Fig. 17. Equivalent circuit for the homogeneous comb structure.

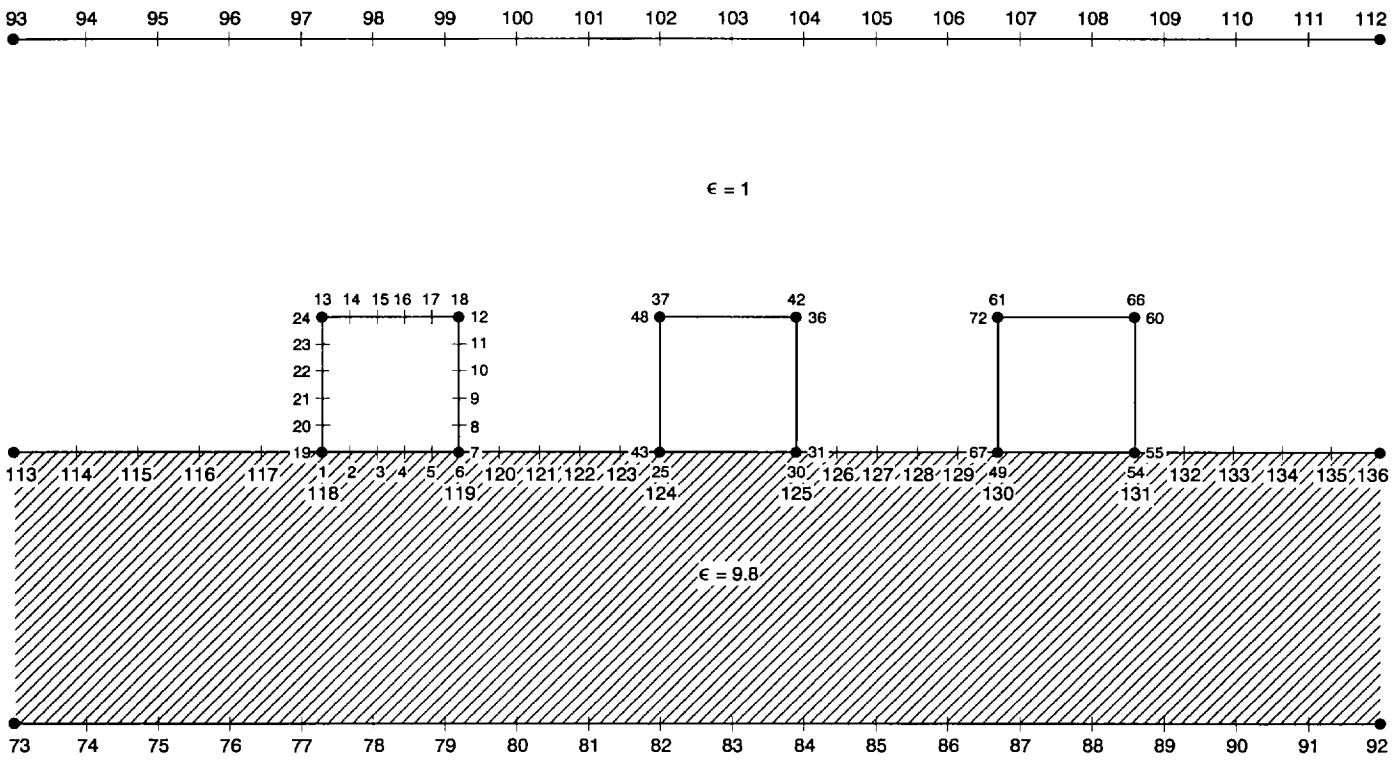

Fig. 18. Location of the nodes used to calculate the capacitance matrix and effective dielectric constant of the partially loaded comb structure.

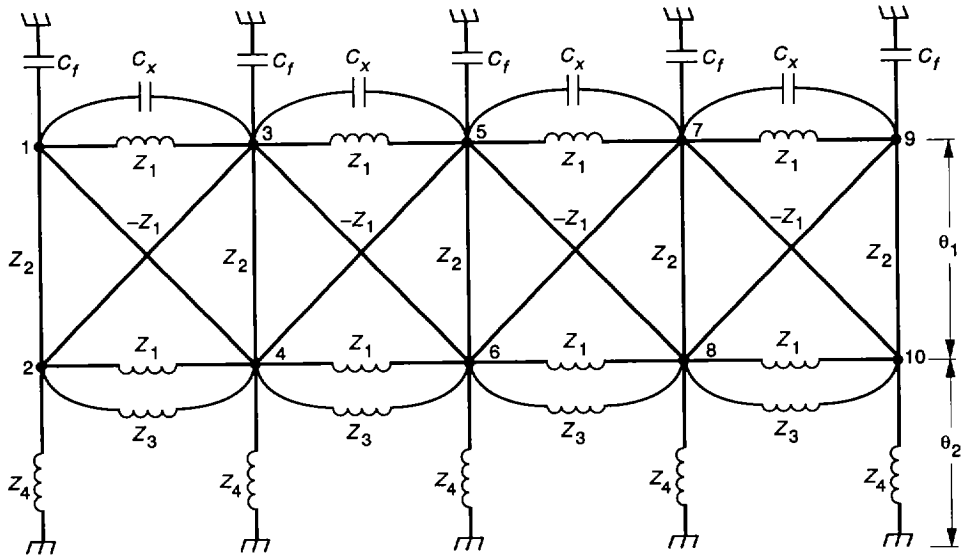

Fig. 19. Equivalent circuit used to model the S-band slow-wave structure of Fig. 16.

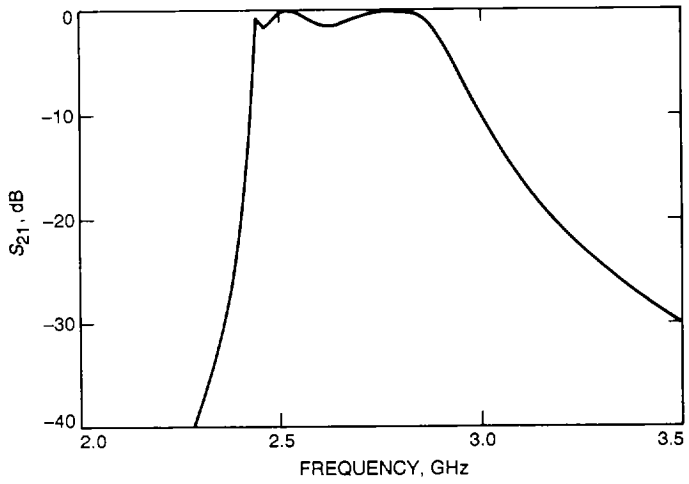

Fig. 20. Calculated S_{21} response for the circuit of Fig. 19.

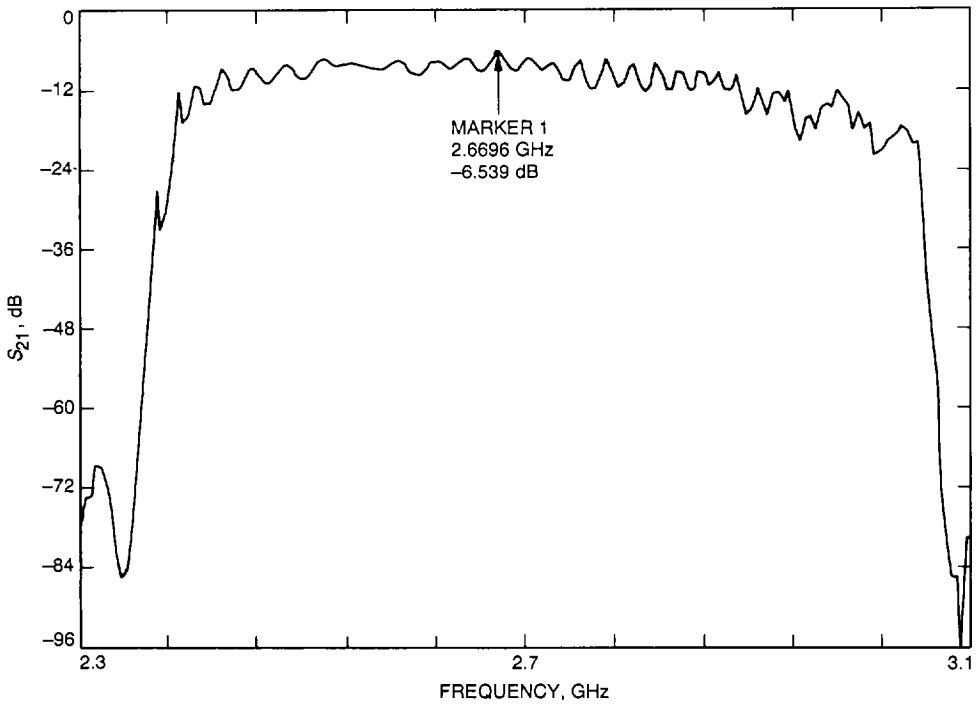

Fig. 21. Measured S_{21} response for the S-band slow-wave structure, which contains 48 fingers.

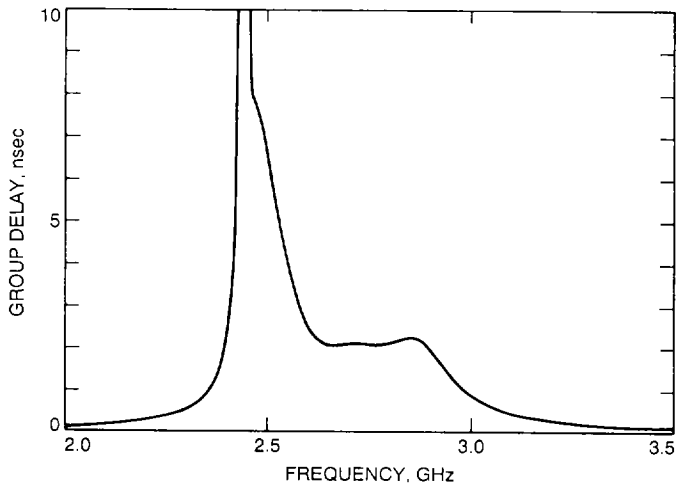

Fig. 22. Calculated group delay for the circuit of Fig. 19.

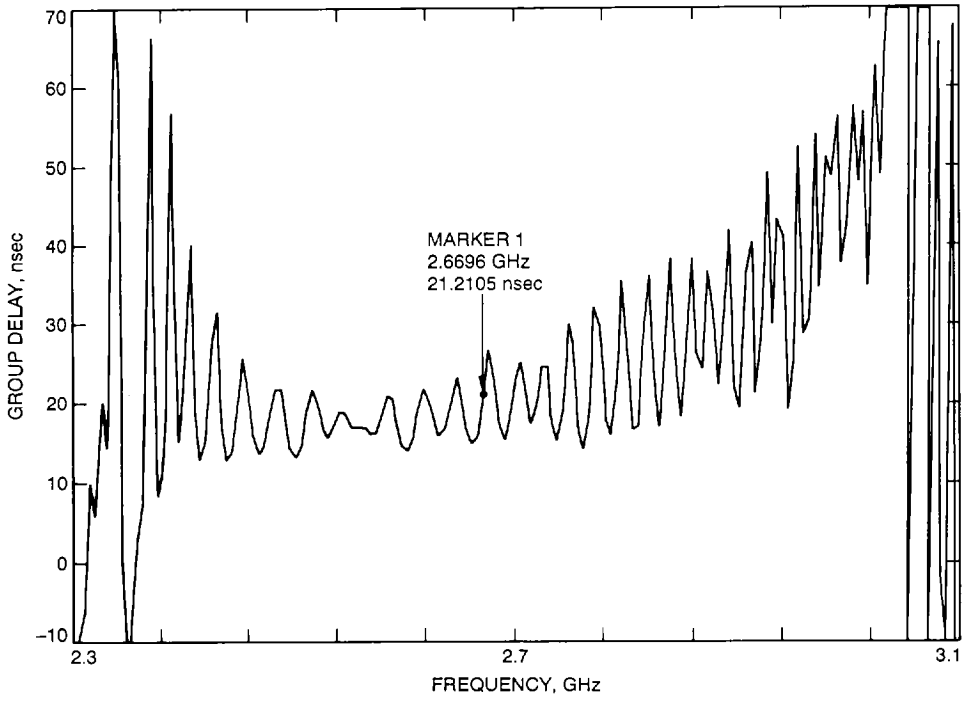

Fig. 23. Measured group delay for the S-band slow-wave structure.

Appendix A

Additional Equivalent Circuits

Several different equivalent circuits for coupled lines using transmission lines have been derived by other researchers. The circuits of Seviora and Sato and Cristal have already been mentioned. The circuit of Seviora can be modified by using the capacitance matrix transformation to yield another circuit, which is discussed by Malherbe [18]. The circuit is shown in Fig. A-1, and in it,

$$Z_1 = \frac{377}{\sqrt{\epsilon_r}} \left\{ \frac{C_{11}}{\epsilon} + \frac{\left(\frac{C_{12}}{\epsilon}\right)\left(\frac{C_{22}}{\epsilon}\right)}{\frac{C_{12}}{\epsilon} + \frac{C_{22}}{\epsilon}} \right\}^{-1} \tag{A-1}$$

$$Z_2 = \frac{377}{\sqrt{\epsilon_r}} \left\{ \frac{\frac{C_{12}}{\epsilon} + \frac{C_{22}}{\epsilon}}{\left(\frac{C_{12}}{\epsilon}\right)^2} \right\} \tag{A-2}$$

$$n = 1 + \frac{\frac{C_{22}}{\epsilon}}{\frac{C_{12}}{\epsilon}} \tag{A-3}$$

The problem of modeling coupled-line networks in an inhomogeneous dielectric medium has also been investigated. The counterpart of the Jones and Bolljahn study (symmetric conductors and homogeneous dielectric material) for the case of inhomogeneous dielectric material (symmetric conductors) was performed by Zysman and Johnson [19].

Cheng and Edwards [20] have shown that the three-transmission-line network of Seviora, if extended to include quasi-TEM coupling, becomes the four-transmission network shown in Fig. A-2. This circuit is being given to improve the modeling of the partially loaded geometry, such as the S-band example considered in this article.

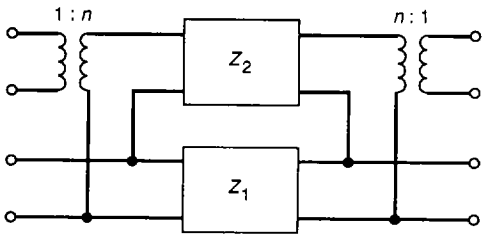

Fig. A-1. Equivalent circuit of Malherbe for coupled lines.

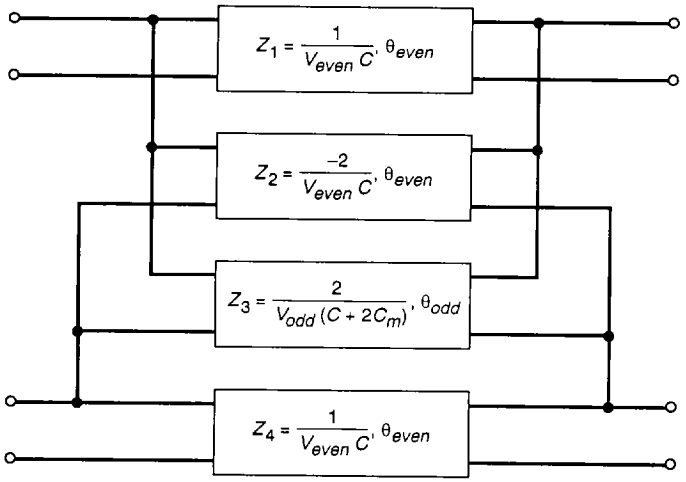

Fig. A-2. Equivalent circuit of Cheng and Edwards to model quasi-TEM coupled lines.

Appendix B

TOUCHSTONE Files

The TOUCHSTONE files used for the X-band and S-band examples described in Section VII are shown in Figs. B-1 and B-2 for reference.

```
DIM

  FREQ GHZ
  RES OH
  IND NH
  CAP PF
  LNG MIL
  TIME NS
  COND /OH
  ANG DEG

VAR
        ZLIN=55.5       !LINE IMPEDANCES CALCULATED FROM CSELF
        ZCRS=-247       !LINE IMPEDANCES CALCULATED
        ZIND=247        !FROM CMUTUAL
        ELIN=150        !ESTIMATED LINE LENGTH
        FLIN=8.0        !AT 8.0 GHZ
        CF1=.1          !FRINGING CAPACITANCE FROM FINGER TIP TO GROUND
        CX1=-.005       !FRINGING CAPACITANCE FROM FINGER TO FINGER

EQN
CKT
        RES   1    0     R=350      !INPUT MATCHING NETWORK
        IND   1    0     L=45
        DEF1P 1          ZIMP

        TLIN  1    2     Z^ZLIN   E^ELIN   F^FLIN
        TLIN  3    4     Z^ZLIN   E^ELIN   F^FLIN
        TLIN  5    6     Z^ZLIN   E^ELIN   F^FLIN
        TLIN  7    8     Z^ZLIN   E^ELIN   F^FLIN
        TLIN  9    10    Z^ZLIN   E^ELIN   F^FLIN
        TLIN  1    4     Z^ZCRS   E^ELIN   F^FLIN
        TLIN  2    3     Z^ZCRS   E^ELIN   F^FLIN
        TLIN  4    5     Z^ZCRS   E^ELIN   F^FLIN
        TLIN  3    6     Z^ZCRS   E^ELIN   F^FLIN
        TLIN  5    8     Z^ZCRS   E^ELIN   F^FLIN
        TLIN  6    7     Z^ZCRS   E^ELIN   F^FLIN
        TLIN  7    10    Z^ZCRS   E^ELIN   F^FLIN
        TLIN  8    9     Z^ZCRS   E^ELIN   F^FLIN
        TLSC  1    3     Z^ZIND   E^ELIN   F^FLIN
        TLSC  2    4     Z^ZIND   E^ELIN   F^FLIN
        TLSC  3    5     Z^ZIND   E^ELIN   F^FLIN
        TLSC  4    6     Z^ZIND   E^ELIN   F^FLIN
        TLSC  5    7     Z^ZIND   E^ELIN   F^FLIN
        TLSC  6    8     Z^ZIND   E^ELIN   F^FLIN
        TLSC  7    9     Z^ZIND   E^ELIN   F^FLIN
        TLSC  8    10    Z^ZIND   E^ELIN   F^FLIN

        CAP   1    0     C^CF1
        CAP   2    0     C^CF1
        CAP   3    0     C^CF1
```

Fig. B-1. TOUCHSTONE file to model the X-band slow-wave structure.

```
        CAP    4      0       C^CF1
        CAP    5      0       C^CF1
        CAP    6      0       C^CF1
        CAP    7      0       C^CF1
        CAP    8      0       C^CF1
        CAP    9      0       C^CF1
        CAP    10     0       C^CF1
        CAP    1      3       C^CX1
        CAP    2      4       C^CX1
        CAP    3      5       C^CX1
        CAP    4      6       C^CX1
        CAP    5      7       C^CX1
        CAP    6      8       C^CX1
        CAP    7      9       C^CX1
        CAP    8      10      C^CX1
        DEF2P  1      9       XTWM

TERM
        XTWM     ZIMP     ZIMP

OUT
        XTWM      DB[S21]  GR1     !PLOTS LOG MAGNITUDE OF S21
        XTWM      DB[S11]  GR2     !PLOTS LOG MAGNITUDE OF S11
        XTWM      TD[S21]  GR3     !PLOTS GROUP DELAY

FREQ
    SWEEP    5.5       9.5       .02

GRID
    RANGE    6.5       9.5       0.5

    GR1    0   -50    10
    GR2    0   -30     5
    GR3    0     5     0.5
```

Fig. B-1 (contd)

```
DIM
  FREQ GHZ
  RES OH
  IND NH
  CAP PF
  LNG MIL
  TIME NS
  COND /OH
  ANG DEG

VAR
        CF1=.0214     !FRINGING CAPACITANCE FROM FINGER TIP TO GROUND
        CX1=.065      !FRINGING CAPACITANCE FROM FINGER TO FINGER
        ELN1=16.5     !LINE LENGTH OF UNLOADED PORTION OF THE FINGER
        ELN2=56       !LINE LENGTH OF LOADED PORTION OF FINGER
        FLIN=2.0      !AT 2.0 GHZ

EQN


CKT
        RES     1   0   R=900
        IND     1   0   L=500
        DEF1P   1       ZIMP

        TLSC    1   3   Z=346      E=ELN1    F=FLIN
        TLIN    1   2   Z=184      E=ELN1    F=FLIN
        TLIN    1   4   Z=-346     E=ELN1    F=FLIN
        CAP     1   0   C=CF1
        CAP     1   3   C=CX1
        TLSC    2   4   Z=346      E=ELN1    F=FLIN
        TLSC    2   4   Z=236      E=ELN2    F=FLIN
        TLSC    2   0   Z=140      E=ELN2    F=FLIN
        TLIN    2   3   Z=-346     E=ELN1    F=FLIN
        TLIN    3   4   Z=184      E=ELN1    F=FLIN
        CAP     3   0   C=CF1
        TLSC    3   5   Z=346      E=ELN1    F=FLIN
        CAP     3   5   C=CX1
        TLIN    3   6   Z=-346     E=ELN1    F=FLIN
        TLSC    4   0   Z=140      E=ELN2    F=FLIN
        TLSC    4   6   Z=346      E=ELN1    F=FLIN
        TLSC    4   6   Z=236      E=ELN2    F=FLIN
        TLIN    4   5   Z=-346     E=ELN1    F=FLIN
        TLIN    5   6   Z=184      E=ELN1    F=FLIN
        CAP     5   0   C=CF1
        TLIN    5   8   Z=-346     E=ELN1    F=FLIN
        TLSC    5   7   Z=346      E=ELN1    F=FLIN
        CAP     5   7   C=CX1
        TLSC    6   0   Z=140      E=ELN2    F=FLIN
        TLSC    6   8   Z=346      E=ELN1    F=FLIN
        TLSC    6   8   Z=236      E=ELN2    F=FLIN
        TLIN    6   7   Z=-346     E=ELN1    F=FLIN
```

Fig. B-2. TOUCHSTONE file to model the S-band slow-wave structure.

```
        TLIN    7    8    Z=184       E^ELN1    F^FLIN
        CAP     7    0    C^CF1
        TLSC    7    9    Z=346       E^ELN1    F^FLIN
        CAP     7    9    C^CX1
        TLIN    7    10   Z=-346      E^ELN1    F^FLIN
        TLSC    8    0    Z=140       E^ELN2    F^FLIN
        TLSC    8    10   Z=346       E^ELN1    F^FLIN
        TLSC    8    10   Z=236       E^ELN2    F^FLIN
        TLIN    8    9    Z=-346      E^ELN1    F^FLIN
        CAP     9    0    C^CF1
        TLIN    9    10   Z=184       E^ELN1    F^FLIN
        TLSC    10   0    Z=140       E^ELN2    F^FLIN
        DEF2P   2    10   STWM2

TERM

     STWM2    ZIMP   ZIMP


OUT
        STWM2   DB[S21]   GR1      !PLOTS LOG MAGNITUDE OF S21
        STWM2   DB[S11]   GR2      !PLOTS LOG MAGNITUDE OF S11
        STWM2   TD[S21]   GR3      !PLOTS GROUP DELAY

FREQ
   SWEEP     2.0      3.5         0.02

GRID
   RANGE     2.0      3.5         0.50

   GR1     0    -40     10
   GR2     0    -30     5
   GR3     0     10     1
```

Fig. B-2 (contd)

References

Some of the articles listed below can be found in the two following reprint collections of IEEE articles dealing with coupled line circuits.

Leo Young, ed., *Microwave Filters Using Parallel Coupled Lines*, Dedham, Massachusetts: Artech House, Inc., 1972 (contains 30 articles).

Leo Young, ed., *Parallel Coupled Lines and Directional Couplers*, Dedham, Massachusetts: Artech House, Inc., 1972 (contains 26 articles).

[1] R. Seviora, "Equivalent Circuit for Parallel Conductor Array," *IEEE Trans. on Microwave Theory and Techniques*, vol. MTT-16, no. 10, pp. 875–877, October 1968.

[2] R. Sato and E. G. Cristal, "Simplified Analysis of Coupled Transmission Line Networks," *IEEE Trans. on Microwave Theory and Techniques*, vol. MTT-18, no. 3, pp. 122–131, March 1970.

[3] H. J. Riblet, "An Explicit Derivation of the Relationships Between the Parameters of an Interdigital Structure and the Equivalent Transmission Line Cascade," *IEEE Trans. on Microwave Theory and Techniques*, vol. MTT-15, no. 3, pp. 161–166, March 1967.

[4] E. M. T. Jones and J. T. Bolljahn, "Coupled-Strip Transmission Line Filters and Directional Couplers," *I.R.E. Trans. on Microwave Theory and Techniques*, vol. MTT-4, no. 2, pp. 75–81, April 1956.

[5] R. J. Wenzel, "The Modern Network Theory Approach to Microwave Filter Design," *IEEE Trans. on Electromagnetic Compatibility*, vol. EMC-10, no. 2, pp. 196–209, June 1968.

[6] R. J. Wenzel, "Exact Design of TEM Microwave Networks Using Quarter Wave Lines," *IEEE Trans. on Microwave Theory and Techniques*, vol. MTT-12, no. 1, pp. 94–111, January 1964.

[7] R. J. Wenzel, "Exact Theory of Interdigital Band-Pass Filters and Related Coupled Structures," *IEEE Trans. on Microwave Theory and Techniques*, vol. MTT-13, no. 5, pp. 559–575, September 1965.

[8] R. J. Wenzel, "Theoretical and Practical Applications of Capacitance Matrix Transformations to TEM Network Design," *IEEE Trans. on Microwave Theory and Techniques*, vol. MTT-14, no. 12, pp. 635–647, December 1966.

[9] A. Djordjevic, R. F. Harrington, T. Sarkar, and M. Bazdar, *Matrix Parameters for Multiconductor Transmission Lines: Software and Users Manual,* Dedham, Massachusetts: Artech House, Inc., 1989.

[10] W. J. Getsinger, "Coupled Rectangular Bars Between Parallel Plates," *IRE Trans. on Microwave Theory and Techniques*, vol. MTT-10, no. 1, pp. 65–72, January 1962.

[11] TOUCHSTONE, EEsof, Inc., 1987.

[12] S. B. Cohn, "Shielded Coupled-Strip Transmission Line," *IRE Trans. on Microwave Theory and Techniques*, vol. MTT-3, no. 5, pp. 29–38, October 1955.

[13] H. E. Green, "The Numerical Solution of Some Important Transmission-Line Problems," *IEEE Trans. on Microwave Theory and Techniques*, vol. MTT-13, no. 5, pp. 676–692, September 1965.

[14] R. E. Diaz, "The Discrete Variational Conformal Technique for the Calculation of Strip Transmission-Line Parameters," *IEEE Trans. on Microwave Theory and Techniques*, vol. MTT-34, no. 6, pp. 714–722, June 1986.

[15] D. W. Kammler, "Calculation of Characteristic Admittances and Coupling Coefficients for Strip Transmission Lines," *IEEE Trans. on Microwave Theory and Techniques*, vol. MTT-16, no. 1, pp. 925–937, November 1968.

[16] C. Wei, R. F. Harrington, J. R. Mautz, and T. K. Sarkar, "Multiconductor Transmission Lines in Multi-layered Dielectric Media," *IEEE Trans. on Microwave Theory and Techniques*, vol. MTT-32, no. 4, pp. 439–450, April 1984.

[17] S. M. Perlow, "Analysis of Edge-Coupled Shielded Strip and Slabline Structures," *IEEE Trans. on Microwave Theory and Techniques*, vol. MTT-35, no. 5, pp. 522–529, May 1987.

[18] J. A. G. Malherbe, *Microwave Transmission Line Filters,* Dedham, Massachusetts: Artech House, Inc., 1979.

[19] G. Zysman and A. K. Johnson, "Coupled Transmission Line Networks in an Inhomogeneous Dielectric Medium," *IEEE Transactions on Microwave Theory and Techniques*, vol. MTT-17, no. 10, pp. 753–759, October 1969.

[20] S. Cheng and M. L. Edwards, "TEM Equivalent Circuits for Quasi-Tem Couplers," *1990 IEEE MTT-S International Microwave Symposium Digest*, vol. 1, IEEE, Piscataway, New Jersey, p. 387, May 1990.